nature communications

Article

https://doi.org/10.1038/s41467-026-70468-2

Genome-centric metagenomics reveals electroactive syntrophs in a conductive particle-dependent consortium from coastal sediments

Received: 12 August 2025

Accepted: 23 February 2026

Published online: 24 March 2026

Check for updates

Danijel Jovicic[1,4], Konstantinos Anestis[1,4], Jacek Fiutowski[2], Bo Barker Jørgensen[3], Kasper Urup Kjeldsen[3] & Amelia-Elena Rotaru[1]

Conductive particles are common in coastal sediments, yet their role in shaping methane-producing communities and pathways remains unclear. We applied genome-resolved metagenomics to a sediment-derived consortium serially transferred for a decade and obligately dependent on granular activated carbon (GAC). We discovered a particle-obligate food web composed of electrogenic syntrophic acetate oxidizers (SAO), an electrotrophic methanogen, and necromass recyclers. The primary SAO electrogen, *Candidatus* Geosyntrophus acetoxidans, represents a new genus and possesses a complete acetate oxidation pathway and extracellular electron-transfer (EET) machinery, including two porin-cytochrome conduits, 43 additional multiheme cytochromes and conductive pili. A secondary SAO, a *Lentimicrobium* sp. with a giant PCC-cluster, supplies an alternative EET-linked acetate-oxidation route. Electrons from electrogens transfer via GAC to a *Methanosarcina* equipped with the heptaheme cytochrome MmcA and flagellin for electron uptake. These results provide a genomic blueprint of this particle-obligate environmental consortium and suggest an overlooked acetate-to-methane electron-transfer route in geoconductor-rich anoxic sediments.

Methane is a potent greenhouse gas with a global warming potential approximately 84-times higher than CO_2 over a 20-year period[1,2]. A considerable fraction of the atmospheric methane is derived from acetate, channeled either through acetoclastic methanogens (Eq. 1) or by syntrophic acetate oxidation (SAO), in which an acetate-oxidizing bacterium supplies reducing equivalents (e.g., H_2 or electrons) to a partner methanogen, rendering acetate oxidation thermodynamically feasible[3,4]. (Eqs. 2–3). Although these reactions operate at the thermodynamic limits of life, SAO is essential in methane-producing ecosystems[5–15].

$$\text{Acetoclastic methanogenesis}: CH_3-COOH \rightarrow CH_4 + CO_2 \quad (1)$$

$$\text{Syntrophic acetate oxidation}: CH_3-COOH + 2H_2O \rightarrow 2CO_2 + [8H^+ + 8e^-] \quad (2)$$

$$CO_2-\text{reductive methanogenesis}: CO_2 + [8H^+ + 8e^-] \rightarrow CH_4 + 2H_2O \quad (3)$$

[1]Department of Biology, Faculty of Natural Science, University of Southern Denmark, Odense, Denmark. [2]Mads Clausen Institute, NanoSYD, University of Southern Denmark, Sønderborg, Denmark. [3]Section for Microbiology, Department of Biology, Aarhus University, Aarhus, Denmark. [4]These authors contributed equally: Danijel Jovicic, Konstantinos Anestis. e-mail: arotaru@biology.sdu.dk

SAO-driven methane formation occurs across different anoxic environments including anaerobic digesters[5–8], rice paddies[9–11] and freshwater or marine sediments[12–15]. In coastal settings, natural and climate driven erosion mobilizes terrigenous material[16], such as iron oxides (e.g., magnetite)[17,18] and wildfire-derived char particles[19–21] that act as semiconducting conduits[22]. Laboratory studies show that such particles or their analogs (i.e., granular activated carbon, an analog for chars) can raise methane production up to 15-fold by serving as electrical conduits for CIET (Conductive particle mediated Interspecies Electron Transfer) between electrogenic bacteria and electrotrophic methanogens in synthetic consortia[23–27]. We previously observed a similar minimum four-fold stimulation of methane production when conductive particles were supplied from the onset to laboratory enrichments established from aquatic sediments (coastal marine or lacustrine)[15,22]. These incubations led to the enrichment of environmental CIET-SAO consortia[15,22], which could not survive in the absence of conductive particles[15,22]. These particle-dependent partnerships may determine whether acetate (a central intermediate in conversion of organics to methane) is routed to methane via SAO or directly via acetoclastic methanogenesis. Because CIET-SAO remains virtually unreported in situ, and its mechanism remain elusive, these sediment enrichments initiated with conductive particles remain the closest practicable proxy for disentangling how these consortia route acetate to methane and accelerate organic-matter turnover in anoxic soils and sediments[4].

In fact, the first compelling evidence for conductive particle-obligate SAO came from these same enrichments, which we established 10 years ago from coastal Bothnian Bay sediments[15]. When singly methyl-labeled acetate ($^{13}CH_3$-COOH) was supplied, $^{13}CO_2$ accumulated only in GAC-amended bottles demonstrating acetate oxidation by bacteria rather than acetoclastic cleavage by methanogens. In stark contrast, no such accumulation occurred in GAC-free controls. Furthermore, inhibitor tests showed that blocking methanogenesis halted acetate oxidation instantly, confirming a critical co-dependency between bacterial and archaeal partners. Remarkably, the consortium proved GAC obligate: without GAC, methane production plummeted four-fold, with the CIET-SAO partners declining to undetectable levels[15]. Advanced NanoSIMS analyses on these CIET-SAO consortia, demonstrated that over 80% of the ^{13}C-label was incorporated by a bacterium distantly related to *Geobacter*, working in partnership with a *Methanosarcina*-like archaeon. However, 16S rRNA-gene phylogeny and probes alone could not resolve the phylogeny of either organism[15]. The *Geobacter*-far-related bacterium displayed only 95-96.6% 16S rRNA-gene identity to *Geobacter psychrophilus*, a misclassified organism that crosses the boundaries of both the *Geobacter* genus and the *Geobacteraceae* family. The *Methanosarcina* shared 98-99% 16S rRNA-gene identity to both *M. subterranea* and *M. lacustris*. Despite this compelling physiological evidence, the phylogenomic placement, electron-transfer routes, and genomic determinants that enable these electrogenic and electrotrophic partners to thrive on conductive particles remained unresolved. To address this gap, and building on the physiological findings of Rotaru et al.[15], this study aims to resolve the genomic blueprint of that same particle-bound consortium, identify the electroactive microorganisms, and resolve their capabilities for metabolic cross-feeding via conductive particles.

In this work we applied long-read, genome-centric metagenomics to the above Bothnian Bay consortium serially propagated for a decade on GAC. We recovered 24 metagenome assembled genomes (MAGs), including near-complete genomes of electrogens and *Methanosarcina* partners alongside other coexisting taxa. We could identify the conductive-particle-linked electron-transfer machinery and reconstruct the metabolic network that channels acetate to methane. These results provide a genomic blueprint of a conductive particle-obligate SAO consortium and a foundation for assessing how natural and anthropogenic conductive particles could amplify methane emissions in coastal marine environments.

Results and discussion

To determine the molecular basis of CIET in an environmental conductive particle−obligate SAO consortium, we first re-confirmed its physiology. After a decade of serial transfers with GAC, the Bothnian Bay SAO consortium continued to oxidize acetate at 0.5 ± 0.1 mM day^{-1} and produce 0.2 ± 0.0 mmol CH_4 day^{-1}, matching previously reported rates[15] (Fig. 1a). By contrast, a parallel line of serially transferred GAC-free controls remained virtually inactive over the 42-day incubation period (acetate: 0.01 ± 0.09 mM day^{-1}; methane: 0.01 ± 0.02 mmol day^{-1}) (Fig. 1b), confirming that the electrically conductive scaffold provided by GAC remains indispensable for SAO after a decade of serial cultivation and enrichment.

Helium-ion micrographs of GAC-particles (Fig. 1c–e, Supplementary Figs. S1, S2) revealed round *Methanosarcina*-like cells (M) interspersed among rod-shaped bacterial partners (B) without consistent cell-to-cell contact, supporting the notion that electrons are exchanged via the conductive matrix rather than through direct cell-to-cell contact.

To assess the identity of the electrogenic SAO-bacteria and electrotrophic methanogenic partner that continued to inhabit GAC-particles after a decade of sediment free serial propagation, we performed metagenomic profiling of the GAC-obligate microbiome. Our analysis revealed indeed a MAG distantly related to *Geobacter* accounting for 9.4% of the total reads, along with a *Methanosarcina*-related MAG that represented 12% of the total reads. The 16S rRNA-gene of these two MAGs matched (~99% and above) the previously reported 16S-rRNA phylotypes[15]. Both these MAGs were essentially absent from GAC-free controls (<0.1%; Fig. 2a, Supplementary Fig. S3). These results are consistent with our earlier stable isotope labeling studies that identified a *Geobacter*-like organism as the dominant acetate oxidizer (incorporating >80% of the labeled acetate) and a *Methanosarcina* as the sole methanogen in the consortium[15].

In this study, we reconstructed high-quality MAGs (>97% completeness, <0.7% contamination) for the key syntrophic partners, *Geobacter*-like and *Methanosarcina*-like microorganisms (Fig. 2a). Beyond these core SAO partners, GAC also enriched specifically the relative abundance of three other species – belonging to *Sedimentibacter* (6.5%), *Lentimicrobium* (3.4%), and *Desulforhopalus* (3%) (Fig. 2a). Given that other representatives of *Sedimentibacter* and *Lentimicrobium* were detected in the metagenomic libraries of both GAC-supplemented and GAC-free controls, we hypothesize that their primary ecological role may not be related to direct electron transfer, but rather to the recycling of organic matter resulting from biomass turnover within the community.

Taken together, the activity profiles, spatial organization and metagenomic data indicate that decade long serial transfers of the consortium did not alter the core partnership between *Geobacter*-like bacteria and *Methanosarcina*-like archaea. So, the Baltic Sea *Geobacter* continued to oxidize acetate and transfer electrons through the GAC matrix, while the Baltic *Methanosarcina* completed the syntrophic process by accepting the electrons from GAC to reduce CO_2 to CH_4.

Ca. Geosyntrophus acetoxidans, the first cultured (non-axenic) representative of the placeholder genus JACRCG01

Despite its stable dominance over a decade of serial transfers, the phylogenetic identity of this *Geobacter*-like bacterium remained unresolved. 16S-rRNA gene phylogeny yielded ambiguous results, placing the Baltic "*Geobacter*" between *Pelobacter chapellei* and *Geobacter psychrophilus* (sharing ~96–97% 16S rRNA gene identity to both, Supplementary Fig. S4). Furthermore, the Genome Taxonomy Database (GTDB) classified this predominant "*Geobacter*"-MAG into an uncharacterized genus level lineage (genus JACRCG01).

https://doi.org/10.1038/s41467-026-70468-2

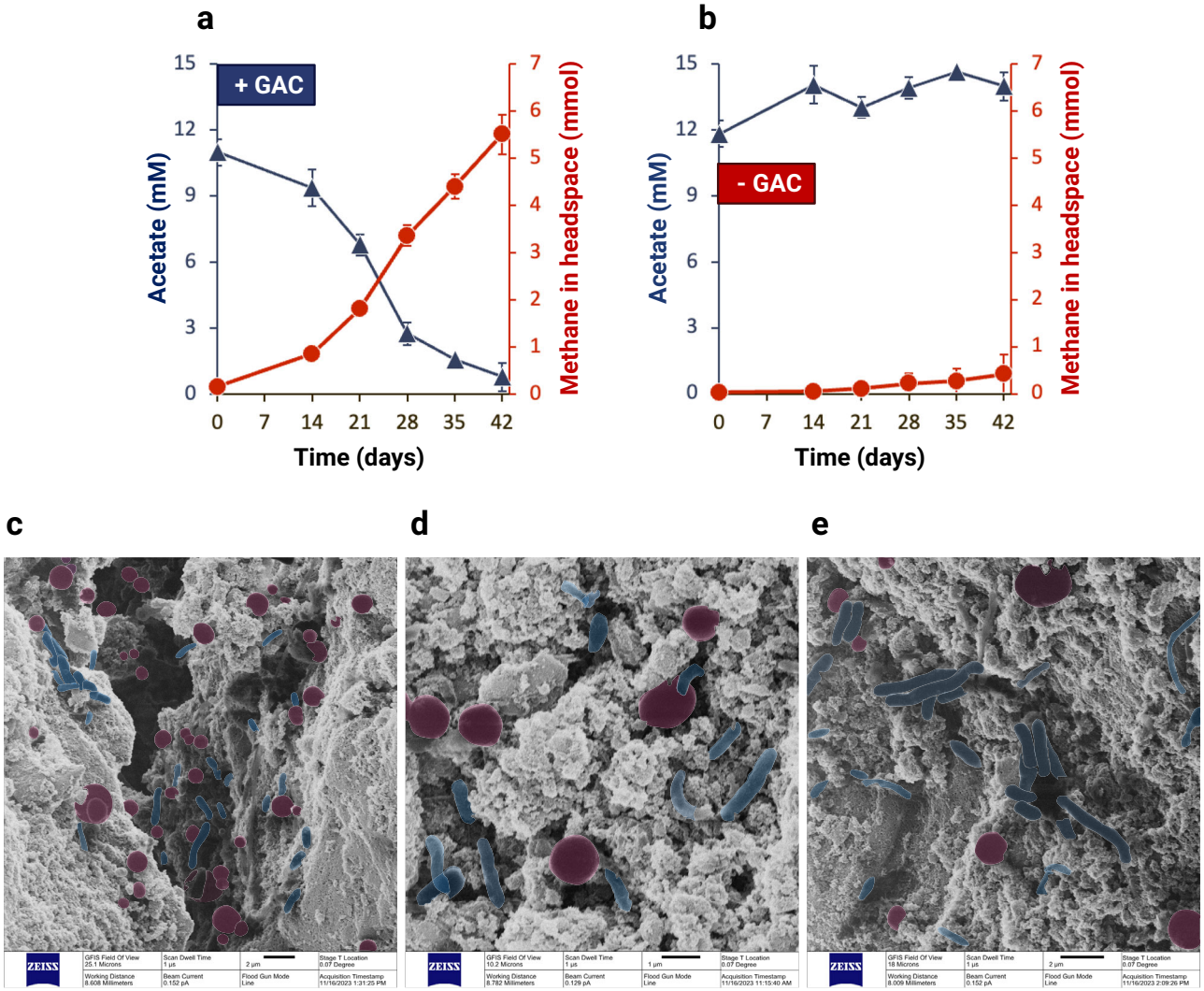

Fig. 1 | Syntrophic acetate oxidation (SAO) by a Baltic Sea consortium dependent on conductive particles. Methane production (●) and acetate consumption (▲) over 42 days in anaerobic cultures incubated **a** with granular activated carbon (GAC) or **b** without GAC; values are means ± SD of biological replicates ($n = 3$ for control without GAC and $n = 6$ for cultures with GAC). **c**–**e** Representative colorized helium-ion microscopy (HIM) micrographs of GAC particles collected at day 42 from three independent biological replicates. 5–9 images were collected per replicate. The images show *Methanosarcina* cells (red, round cells) and associated bacterial partners (blue, long and short rods). Scale bars: 2 µm (**c**, **e**) and 1 µm (**d**). Created in BioRender. Rotaru, A. (2026) https://BioRender.com/jpxdj2c. Additional HIM micrographs are included in Supplementary Figs. S1, S2.

Because no genome information existed for its closest relative, *Geobacter psychrophilus*, we sequenced the genome of the only available strain of this species—*G. psychrophilus* strain P39[28], kindly provided by Prof. D. Lovley (UMass Amherst). Concatenated phylogenomic analysis using 120 marker genes[29] placed the Baltic "*Geobacter*" firmly in a robust clade with *G. psychrophilus* strain P39. Yet their genomic divergence was substantial, sharing only 73.3% average nucleotide identity (ANI) and 68.8% average amino acid identity (AAI) values that fall at the limit of accepted genus thresholds (~75 % ANI, 60–80% AAI, Supplementary Fig. S5)[30,31].

Consistent with a comprehensive reevaluation of the order *Geobacterales* by Xu et al.[30], the Baltic Sea "*Geobacter*" and *G. psychrophilus* clustered within a newly proposed family *Pseudopelobacteraceae*[32], clearly separated from canonical *Geobacter* species of the family *Geobacteraceae* (Fig. 2b). This taxonomic ambiguity within the order *Geobacterales* emphasizes the urgent need for a formal revision. To clearly delineate the Baltic "*Geobacter*" from other *Pseudopelobacteraceae* we propose the name *Ca*. Geosyntrophus acetoxidans (*Candidatus* Ge.o.syn.tro'phus; Gr. n. gē, earth; Gr. adj. syntrophos, feeding together; acetoxidans: N.L. n. acetum, acetate, and N.L. pres. part. oxidans, oxidizing), marking its novelty and ecological specialization.

High quality genome reconstruction (97.9% completeness and 0.7% contamination) of the *Ca*. Geosyntrophus acetoxidans MAG revealed that it encodes the entire toolkit for acetate oxidation and an all-inclusive extracellular electron-transfer (EET) apparatus including conductive pili and 47 multiheme cytochromes (MHCs) (Fig. 3, Supplementary Data Table S1, S2), and the largest MHC repertoire among all the MAGs recovered (Supplementary Fig. S8). The EET apparatus of *Ca*. Geosyntrophus had four modules similar in architecture to those in *Geobacter* species (Fig. 4b and Supplementary Fig. S9); however, almost all MHCs show only low (<30%) to moderate (<60%) amino-acid identity to canonical *Geobacter* homologs (Supplementary Fig. S10), indicative of substantial diversification.

Acetate enters the cell cytoplasm through porins and a cation/acetate symporter (ActP) and it's activated to acetyl-CoA either directly via acetyl-CoA synthetase (Acs) or with intermediate formation of acetyl-phosphate catalyzed by acetate kinase (AckA) and phosphate acetyltransferase (Pta) (Fig. 3). The resulting acetyl-CoA is then

https://doi.org/10.1038/s41467-026-70468-2

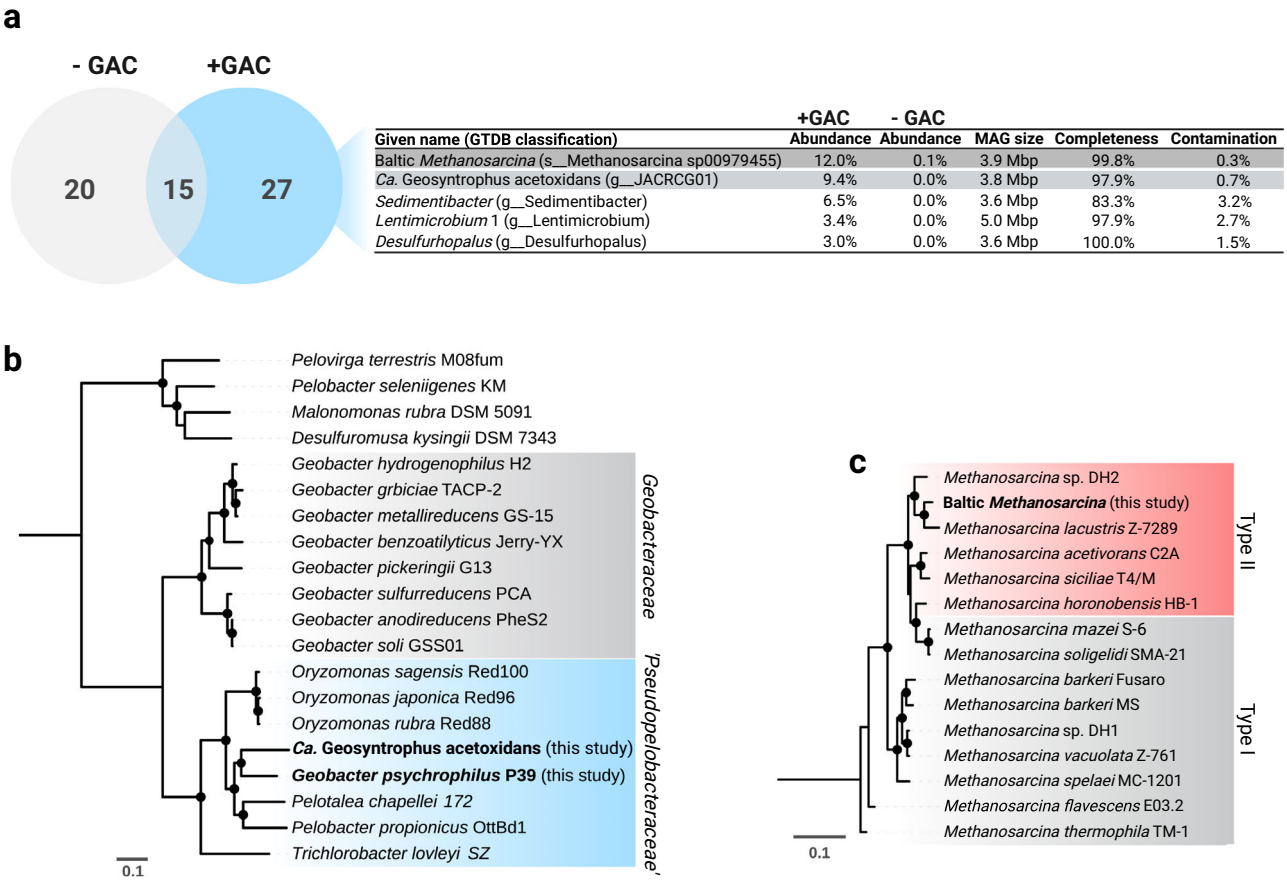

Given name (GTDB classification)	+GAC Abundance	- GAC Abundance	MAG size	Completeness	Contamination
Baltic *Methanosarcina* (s__Methanosarcina sp00979455)	12.0%	0.1%	3.9 Mbp	99.8%	0.3%
Ca. Geosyntrophus acetoxidans (g__JACRCG01)	9.4%	0.0%	3.8 Mbp	97.9%	0.7%
Sedimentibacter (g__Sedimentibacter)	6.5%	0.0%	3.6 Mbp	83.3%	3.2%
Lentimicrobium 1 (g__Lentimicrobium)	3.4%	0.0%	5.0 Mbp	97.9%	2.7%
Desulfurhopalus (g__Desulfurhopalus)	3.0%	0.0%	3.6 Mbp	100.0%	1.5%

Fig. 2 | Phylogenomic placement of the key players in a Baltic Sea syntrophic acetate oxidizing consortium dependent on GAC. a Venn diagram showing MAGs unique to particle-free controls (−GAC, gray), unique to GAC-amended cultures (+GAC, blue) or shared between both (overlap). The table lists the five most abundant MAGs in the GAC-amended incubations with their GTDB affiliation, relative abundance, genome size, and quality metrics. **b** Maximum likelihood phylogenomic tree based on a concatenated alignment of 120 GTDB marker proteins. The tree was inferred using RAxML-HPC2 with the PROTCAT + DAYHOFF model and 100 bootstrap replicates. The Baltic electrogen previously listed as a Baltic 'Geobacter' here re-named *Ca.* Geosyntrophus acetoxidans (bold) and *Geobacter psychrophilus* P39 (genome sequenced in this study, bold italics) form a clade within the family 'Pseudopelobacteraceae' (blue shading), clearly delineated from Geobacteraceae (gray shading). **c** Corresponding archaeal tree based on 53 archaeal marker genes. The Baltic *Methanosarcina* (bold) groups with type II strains (red shading) and is distinct from type I lineages (gray shading). For **b**, **c**, filled circles mark bootstrap support above 70 % for 100 replicates. Scale bar, 0.1 substitutions per site. Created in BioRender. Rotaru, A. (2026) https://BioRender.com/f25a381. Distribution of the MAGs identified under GAC and particle-free incubations can be found in Supplementary Fig. S3.

completely oxidized via a complete tricarboxylic acid cycle (TCA), generating NADH and $FADH_2$. NADH feeds electrons to the membrane-bound NADH-quinone oxidoreductase reaching the menaquinone pool and driving proton translocation. $FADH_2$ generated by succinate dehydrogenase funnels also electrons from TCA to the menaquinone pool. From menaquinol, electrons could pass to nine inner-membrane MHCs—including ImcH/CbcL homologs and enter a densely populated periplasm containing 28 MHCs (Fig. 3, Supplementary Data Tables S1, S2). Two of the periplasmic MHCs share moderate (~45%) amino acid identity with well described PpcA/PpcD redox hubs of *Geobacter* spp.[33,34], reflecting functional convergence despite distant phylogeny.

Periplasmic electrons exit through two porin-cytochrome-cytochrome (PCC3 architecture) conduits conserved among *Desulfuromonadales*, OmbB-OmaB-OmcB and ExtEFG[35]. Both PCCs are essential for extracellular electron transfer in *Geobacter*, where their deletion abolishes electron flow[35,36]. In *Ca.* Geosyntrophus, both PCCs mirrored the gene organization of *G. sulfurreducens* PCCs[35], a porin followed by a periplasmic facing MHC (penta- or octaheme) and an outer-membrane duodecaheme MHC (Fig. 4). However, the outer-membrane cytochrome of the ExtEFG-module in *Ca.* Geosyntrophus contains twice as many canonical heme-binding motifs (24 CXXCH), or 36 predicted heme sites when including non-canonical motifs ($CX_{n=2-15}CH/K$, Supplementary Data Table S2) placing it among the largest MHCs predicted in *Desulfuromonadales*[37]. Despite their conserved organization, both PCCs share only 36–57% amino-acid identity with *G. sulfurreducens* orthologs (Fig. 4b, Supplementary Data Table S2). This divergence aligns with the elevated evolutionary rates of surface-exposed MHCs (Fig. 4a) and with broader observations that cell-surface proteins evolve faster than proteins from other cellular compartments[38,39], reflecting adaptive diversification in response to variable extracellular environments[39].

Beyond these two syntenic PCC modules, two additional syntenic MHC-containing modules were identified (Supplementary Fig. S9). Most other MHCs did not cluster into modules and instead displayed mosaic origins, sharing similarity with MHCs from diverse iron- and sulfate-reducing taxa (Supplementary Data Table S2). This pattern suggests that MHC evolution in *Ca.* Geosyntrophus occurred via modular pruning and grafting of protein modules and horizontal gene transfer, a process reported for EET associated MHCs[40]. Together these features support a mosaic rather than strictly vertical inheritance of EET components.

Beyond the outer membrane, electrons may be relayed either by four extracellular MHCs that can polymerize into nanowires[41] and/or by two PilA monomers whose aromatic-residue pattern is identical to

https://doi.org/10.1038/s41467-026-70468-2

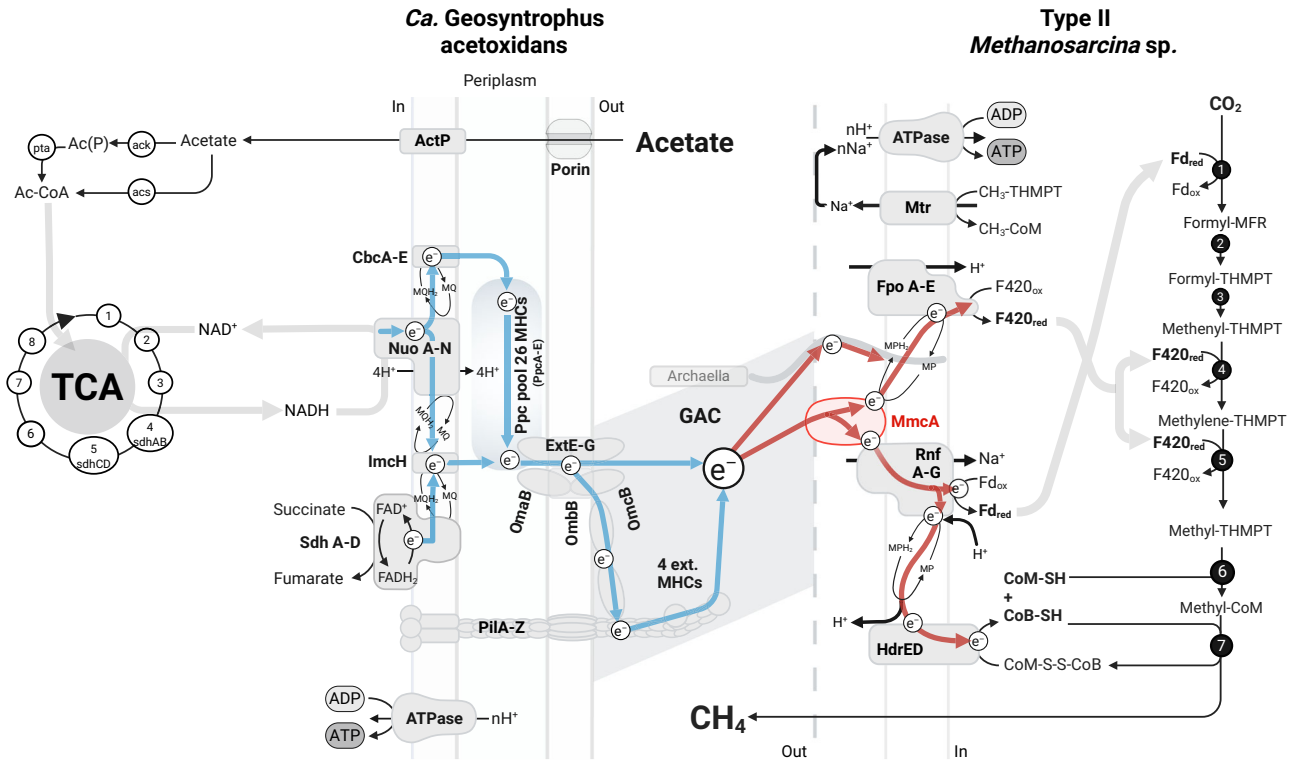

Fig. 3 | Proposed electron-transfer network for syntrophic acetate oxidation using GAC. The metabolic reconstruction incorporates high-quality MAGs of *Ca.* Geosyntrophus acetoxidans (left, blue) and Baltic type II *Methanosarcina* sp. (right, red). In *Ca.* Geosyntrophus acetoxidans, acetate is imported and activated to acetyl-CoA, which is fully oxidized in the TCA cycle, producing NADH and $FADH_2$. Electrons from these cofactors enter the menaquinone pool via NADH dehydrogenase (Nuo) and succinate dehydrogenase (Sdh), flowing through inner-membrane MHCs to a periplasmic reservoir before exiting the cell via two PCC-conduits (Omb/a/cB and/or ExtEFG). Extracellular MHCs and conductive e-pili transfer electrons to GAC, which then reach the methanogen. Electrons from GAC arrive at the outer-surface of the methanogen to reach the MHC MmcA or, secondarily, at an archaellum-associated route (gray wire-like). MmcA contributes electrons to reducing the methanophenazine (MPH_2) pool, bifurcating electrons to the Rnf complex and $F_{420}H_2$ dehydrogenase. Besides ferredoxin, Rnf also supplies electrons to heterodisulfide reductase, regenerating reduced Coenzyme M and Coenzyme B. The TCA-cycle and the CO_2-reductive methanogenesis pathway involve several enzymes, all encoded in the MAGs of *Ca.* Geosyntrophus acetoxidans and Baltic *Methanosarcina*, respectively. Reactions 1–7 for CO_2-reductive methanogenesis: (1) CO_2-activation by methanofuran, (2) formyl transfer to tetrahydromethanopterin (H_4MPT), (3) cyclization to methenyl-H_4MPT, (4) reduction to methylene-H_4MPT, (5) further reduction to methyl-H_4MPT, (6) methyl transfer to coenzyme M, (7) final reduction of methyl-coenzyme M to methane. Created in BioRender. Rotaru, A. (2026) https://BioRender.com/844qy3r. For additional information see Supplementary Data Tables S1, S3.

that of the conductive pili of *G. metallireducens* (11.5% aromatics; Fig. 4). Previously, it was shown that the aromatic amino acid distribution is essential for electron delocalization and long-range conductivity[42,43]. Also, deletion of the *pilA* gene abolished DIET between *Geobacter* and a type II M*ethanosarcina* (*M. acetivorans*) and GAC could compensate for this loss suggesting that the role of pili in the interaction with GAC and the methanogenic partner is not crucial[44].

Taken together, these data indicate that *Ca.* Geosyntrophus acetoxidans oxidizes acetate and disposes of the resulting electrons through an EET conduit composed of inner membrane multiheme cytochromes, periplasmic MHCs, two porin-cytochrome conduits, and pili. Electrons leaving the MHC-rich periplasm are exported via the PCC conduits and then relayed by four extracellular MHCs and pili to the conductive GAC surface. Unlike canonical *Geobacter* species, which encode four to five PCC sets to engage diverse electron acceptors or partner cells in a changing environment[35,45,46], *Ca.* G. acetoxidans relies on only two. This reduced redundancy is sufficient for CIET, but likely limits alternative strategies such as direct cell-to-cell exchange, which may explain why the *Ca.* Geosyntrophus-*Methanosarcina* consortium failed to persist in the absence of conductive particles[15]. Originating from the conductive-particle-rich, relatively stable, deeply anoxic sediments of the Bothnian Bay, *Ca.* Geosyntrophus may have lost redundant EET pathways as an adaptation to its stable niche.

Methanogenic partner is a type II *Methanosarcina* species

Phylogenomic analysis of 53 concatenated archaeal marker genes place the Baltic Sea *Methanosarcina* MAG within the Type II (non-H_2-utilizing) *Methanosarcina* clade[47], next to *M. lacustris* and *Methanosarcina sp.* DH2 (Fig. 2c). Whole genome comparison shows only 89% ANI and 85.2% AAI to its nearest relative, *M. lacustris* (Supplementary Fig. S7), well below the ~95% ANI species boundary, supporting that it represents a new species of *Methanosarcina*.

This *Methanosarcina* MAG is near-complete (99.8 % completeness, <0.3 % contamination) and encodes the full suite of methanogenic pathways (acetoclastic, methylotrophic and CO_2-reducing) together with components linked to extracellular electron uptake (a multiheme cytochrome MmcA and archaella). As expected for Type II Methanosarcina, it lacks the energy-converting hydrogenase (Ech-type)[47], but carries the sodium-pumping Rnf complex (*rnfABCDEG*), which, together with the membrane-bound $F_{420}H_2$ dehydrogenase (*fpoABCDHIJKLMN*) and heterodisulphide reductase (*hdrDE*) support DIET-driven CO_2-reduction in type II *Methanosarcina*, such as *M. acetivorans*[44,48] (Supplementary Data Table S3). The electron-uptake machinery (MmcA and archaella) (Fig. 5) was similar to that implicated in DIET in *M. acetivorans*[44]. Thus, this Baltic methanogen exhibits the characteristic bioenergetic architecture associated with extracellular electron uptake in type II *Methanosarcina*.

https://doi.org/10.1038/s41467-026-70468-2

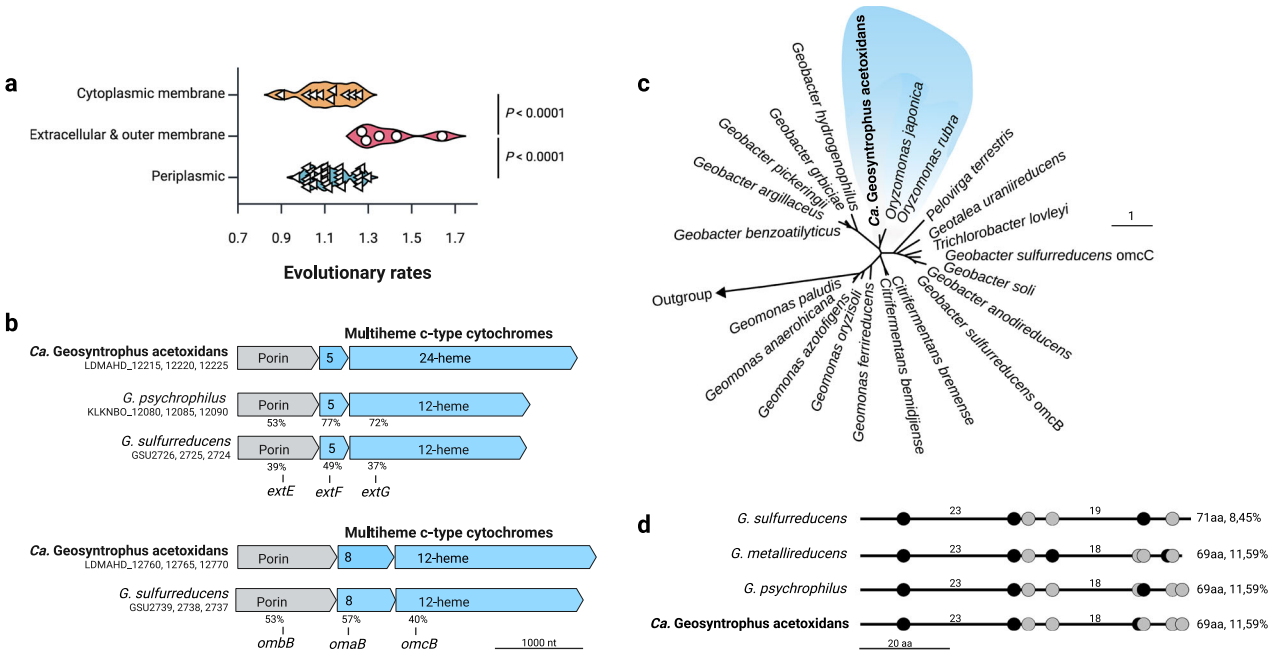

Fig. 4 | Comparative architecture and rates of evolution of outer-surface EET conduits in *Ca.* Geosyntrophus acetoxidans. a Evolutionary rate estimates from OrhtoDB. Values <1 indicate conserved genes, whereas values >1 reflect more rapidly evolving loci. Extracellular and outer membrane MHCs showed significantly higher evolutionary rates than periplasmic or cytoplasmic membrane ones. ($n = 9$ cytoplasmic membrane MHCs, $n = 5$ extracellular MHCs, $n = 28$ periplasmic MHCs). Statistical significance was assessed using one-way ANOVA followed by Tukey's multiple-comparisons test (two-sided). **b** Organization of two Porin-Cytochrome-Cytochrome (PCC) gene clusters in *Ca.* Geosyntrophus acetoxidans, its closest relative *G. psychrophilus* and the model *Geobacter* species *G. sulfurreducens*. *G. psychrophylus* did not harbor the second PCC-module. Percentage values indicate amino acid sequence identity between *Ca.* Geosyntrophus acetoxidans and *G. psychrophilus* or *G. sulfurreducens*. **c** Maximum likelihood phylogeny of OmcB amino acid sequences from representative Geobacterales. The tree was inferred using RAxML-HPC2 on the CIPRES Science Gateway, based on protein alignments (1323 aligned amino acids) using the PROTCAT + DAYHOFF model with 100 bootstrap replicates. The OmcB of *Ca.* G. acetoxidans (blue shading) forms a well-supported clade with other 'Pseudopelobacteraceae', clearly separate from the Geobacteraceae core. Scale bar: 1 amino acid substitution per site. **d** Aromatic residue spacing within PilA monomers forming conductive e-pili. Tyrosines in black (Y) and phenylalanines in gray (F) are indicated along the sequence. *Ca.* Geosyntrophus acetoxidans PilA replicates the aromatic amino acid pattern and spacing in the highly conductive *G. metallireducens* PilA. Values to the right indicate total length (aa) and percentage of aromatic amino acid residues. Scale bar, 20 aa. Created in BioRender. Rotaru, A. (2026) https://BioRender.com/wh2qi6n. Additional details about MHCs per MAG are provided in Supplementary Fig. S8; comparison of PilA aromatic amino acid patterns across 18 species can be found in Supplementary Fig. S11.

The MmcA, also known as the methanogenesis hepta-heme cytochrome, is a well-characterized bidirectional redox conduit[49] indispensable for extracellular electron uptake in type II *Methanosarcina*[44,50]. In *M. acetivorans mmcA* expression increases 4–5-fold when receiving electrons from partner cells or Fe^0 compared to soluble-substrate controls[44,50], and *mmcA* deletion abolishes extracellular electron transfer while leaving growth on soluble substrates intact[44,49,50]. Because *mmcA* is both necessary and strongly induced during EET, it could be considered a potential functional marker for EET in type II *Methanosarcina*, pending broader experimental validation across the clade. In addition, the *Methanosarcina* MAG encodes two complete archaella operons (Fig. 5c), including flagellin homologs to *M. acetivorans*' FlaB1 and FlaB2 (>60% amino acid similarity). Archaella may provide an alternative electron uptake route, although they became dispensable when conductive particles were available[44]. The presence of *mmcA* and archaella operons in our Baltic *Methanosarcina* therefore denotes clear genomic potential to carrying extracellular electron uptake.

Although the Baltic Sea Methanosarcina MAG encodes the full pathways for acetoclastic methanogenesis, our previous physiological tests showed that, without a syntrophic partner, this methanogen was a poor acetate utilizer[15]. Consistent with its genomics makeup and the substrate preferences typical of Type II *Methanosarcina*, it also cannot use hydrogen as an electron donor[48]. This restricted substrate range was further supported by parallel incubations initiated with Fe^0 (run alongside GAC incubations from the same sediment slurry), which enriched for the same *Methanosarcina* species (≥99% rRNA-gene sequence identity to the GAC-derived *Methanosarcina*)[51]. When this Fe^0 -enriched *Methanosarcina* was tested on individual substrates, it failed to grow on H_2 or acetate but grew robustly on Fe^0[51]. Together, these results show that Baltic Methanosarcina is primarily reliant on electron uptake, whether from Fe^0 or GAC[51] rather than from conventional soluble electron donors.

This *Methanosarcina* MAG, specific to GAC incubations, contains the full genetic make up for extracellular electron uptake and CO_2 reductive methanogenesis (Fig. 3, Supplementary Data Table S3). We propose the following working model: each four (of the eight) electrons liberated from acetate oxidation by *Ca.* Geosyntrophus acetoxidans are delivered to GAC, accepted by the outer-surface MHC, MmcA, and then bifurcated. Two electrons reach the Rnf complex generating reduced ferredoxin; the other two enter the methanophenazine pool to fuel a reverse-running Fpo that reduces F_{420} while importing protons. Although reversal of the Fpo consumes the proton gradient, this investment is counterbalanced later in the pathway: the Na^+-pumping methyltransferase Mtr exports Na^+ during the methyl-THMPT→methyl-CoM step, and the membrane-bound HdrDE reduces CoM-S-S-CoB via the methanophenazine pool with scalar H^+ release to the periplasm-like space, rebuilding the ion motive force[48] (Fig. 3). Thus, the extracellular electrons reduce all carriers (ferredoxin and F_{420}) necessary to initiate CO_2 reduction to methane, while Rnf simultaneously supplies electrons to HdrDE to generate reduced CoM and CoB for the terminal step of the CO_2-reductive methanogenesis pathway. The regenerated $\Delta\mu H^+/\Delta\mu Na^+$ then drives the ATP synthase, which can use either H^+/Na^+ ion in *Methanosarcina*[48].

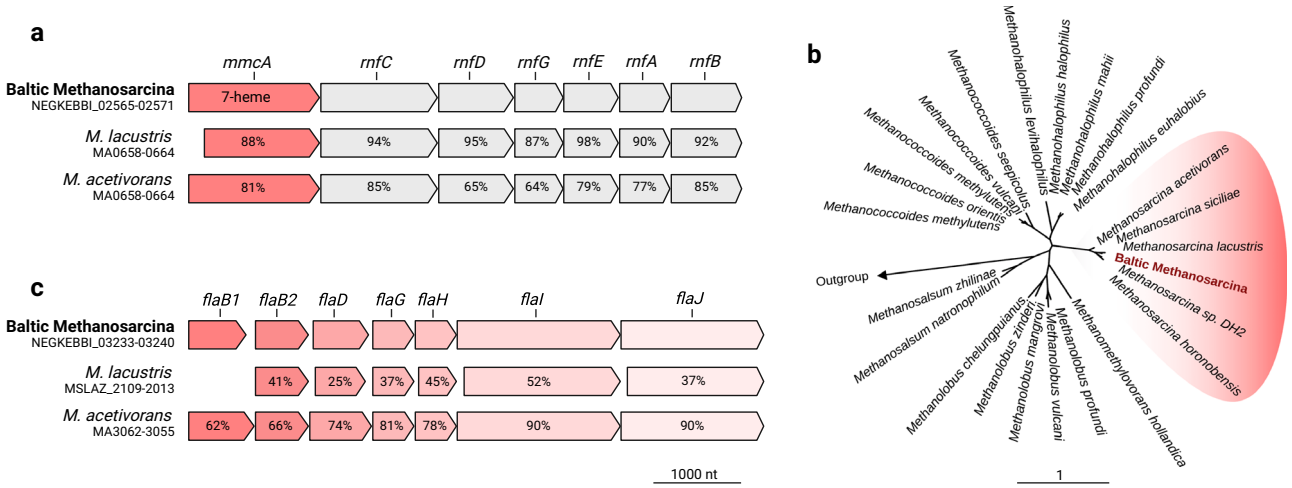

Fig. 5 | Electron-uptake machinery in the Baltic Sea type II *Methanosarcina*. **a** Gene neighborhood of the *mmcA*-electron-transfer locus (*mmcA–rnfCDEGAB*) in the Baltic *Methanosarcina* compared to three reference type II strains. Arrows indicate ORF orientation; numbers inside *mmcA* denote either predicted heme-binding motifs or percentage amino acid identity. **b** Maximum-likelihood tree of MmcA aminoacid sequences from Baltic *Methanosarcina* (bold red) clusters with other type II *Methanosarcina* homologs (red shading) and is clearly separated from MmcA-like cytochromes in other methanogens. Scale bar applies to both **a** and **b** and is 1 kb. **c** Schematic comparison of the complete archaella operon (archaeal flagellum) in the Baltic *Methanosarcina* genome versus *M. acetivorans*; both operon copies are conserved in gene content and length (gray arrows), supporting the potential for an auxiliary, archaella-based electron-uptake route. Scale bar, one amino acid substitution per site. *Created in BioRender. Rotaru, A. (2026)* https://BioRender.com/qgbqwsv.

Auxiliary taxa may engage in biomass turnover or a share of the acetate oxidation

Although *Ca*. Geosyntrophus acetoxidans and the Baltic Type II *Methanosarcina* dominate the GAC-attached consortium, members of three auxiliary lineages, *Sedimentibacter*, a *Desulforhopalus* and a *Lentimicrobium*, were abundant in the GAC-incubations (Fig. 2a). Various other *Sedimentibacter* and *Lentimicrobium* MAG-variants were also well represented in particle-free controls (Supplementary Fig. S3), suggesting that these taxa are unlikely to play a role in interactions with the conductive particles.

Sedimentibacter (6.4% of the reads in GAC-incubations) are well-known fermenters in methanogenic environments[52–54] and were present in acetate-fed microbial fuel cells[55]. However, *Sedimentibacter* have, to date, not been implicated in extracellular electron transfer or SAO. We therefore ascribe their enrichment to turnover of cellular detritus released from the core CIET partnership rather than to direct involvement in extracellular electron flow.

Desulforhopalus (3% of the metagenomic reads in GAC-incubations) was unique to GAC incubations. Although species of *Desulforhopalus* can act as incompletely oxidizing sulfate reducers[56], a sulfate reducing lifestyle is not favored by the conditions provided by our SAO medium lacking sulfate. Besides, the absence of acetate transporters suggests that it is not involved in acetate uptake for subsequent oxidation. If acting as an incomplete oxidizer, any acetate formed intracellularly can still be released via passive diffusion of the protonated form (acetic acid) and/or broad specificity monocarboxylate transporters, so the absence of dedicated acetate importers does not prevent acetate export. In our system, *Desulforhopalus* may be involved in organic matter fermentation. For example, species of *Desulforhopalus* like *D. singaporensis* have been shown to ferment taurine or pyruvate[57], which provides them with an independent carbon- and energy-acquisition route that does not require participation in extracellular electron transfer. Besides, our *Desulforhopalus* MAG lacked PCCs, although it contained an unusually long pilA-like gene whose aromatic residue pattern matches that of conductive e-pili. However, with an incomplete EET machinery and lacking acetate transporters, *Desulforhopalus* is unlikely to be involved in SAO but may be involved in biomass turnover like *Sedimentibacter*.

A single *Lentimicrobium* MAG (3.4% of the metagenomic reads) was recovered only from GAC incubations. A second, closely related *Lentimicrobium* (with 98.6% 16S-rRNA gene identity) appeared also in particle-free controls suggesting that the *Lentimicrobium* lineage is not restricted to conductive-particle conditions (Supplementary Fig. S3). The GAC-specific *Lentimicrobium* MAG encodes 15 MHCs, including a gigantic porin–multiheme cytochrome cluster containing two adjacent MHCs with 61 and 20 predicted heme sites, and lacking synteny to any characterized PCC modules. Its MAG also encodes the complete acetate uptake and utilization pathway (*actP, ack, pta, acs*). Members of Lentimicrobiaceae are typically acetogenic carbohydrate fermenters[58], yet stable-isotope probing has demonstrated acetate assimilation by Lentimicrobiaceae in anaerobic digesters[59,60], pointing to the possibility that this lineage may engage in SAO under certain conditions.

Our previous work showed that a far related *Geobacter* (now identified as *Ca*. Geosyntrophus acetoxidans) was the dominant SAO-bacterium incorporating ~81% of ^{13}C-labeled acetate during mid-exponential growth[15]. In this study, the *Ca*. Geosyntrophus MAG remained the second most abundant genome in incubations with GAC. By contrast, the persistence of *Lentimicrobium* species in both fast-metabolizing GAC incubations and slow-metabolizing particle-free controls points to a different ecological strategy, likely involving lower acetate uptake kinetics and an ability to persist without a conductive scaffold. *Lentimicrobium* may sustain its activity via DIET with methanogens or by fermentatively recycling organic intermediates released within the consortium.

Conductive particles determine consortium stability

Our earlier physiological investigation demonstrated that the SAO consortium was dependent on conductive particles, as removal of the particles (either from the start or after 6 successive transfers) led to major loss of methanogenic activity and a decline of the syntrophic partners[15]. Here we show that this metabolic partnership can also not be maintained long term at the genomic level without conductive particles. After 30 successive transfers without GAC, only minimal methane formation was observed (Fig. 1b), fermentative taxa dominated (*Sedimentibacter*, *Lentimicrobium* and *Humidesulfovibrio;*

Supplementary Fig. S3), *Ca*. Geosyntrophus was undetected, while archaeal populations diminished below 0.5%, with the *Methanosarcina* MAG becoming nearly absent (0.06%, Fig. 2a). In these particle-free lines, abundant fermentative taxa likely scavenged lysis products from transient populations unable to sustain effective methanogenic growth. Together these results indicate that without conductive particles the electrogenic syntroph and their methanogenic partner cannot persist over extended propagation periods.

Partnerships based on direct interspecies electron transfer (DIET) involved in methane production have been documented mainly in synthetic co-cultures assembled in the laboratory, whose activity was promoted by conductive particles through conductive particle mediated interspecies electron transfer (CIET). None of these synthetic consortia require conductive particles for survival[23–26,61]. The Baltic Sea consortium represents the only naturally occurring particle-obligate syntrophy that has been maintained and studied in the laboratory. Its obligate reliance on conductive particles[15], highlights an ecological strategy in which co-existing electroactive bacteria and electrotrophic methanogens exploit environmentally available geoconductors to exchange electrons, a mechanism likely widespread, but largely overlooked in energy-limited, geoconductor-rich sediments and subsurface environments.

The genomic analyses presented here offer a possible explanation for this conductive particle dependence. *Ca*. Geosyntrophus acetoxidans, carries a streamlined EET machinery (two PCC conduits and 47 MHCs), in contrast to the more redundant systems of canonical *Geobacter* species (~four-five PCC conduits and ~127 MHCs per genome)[62,63]. In *Geobacter*, such redundancy supports versatility and rapid adjustment to changing conditions, for example by deploying specialized PCCs matched to different extracellular electron acceptors[35,46]. By contrast, the minimal EET-conduit architecture of *Ca*. Geosyntrophus (reduced PCC and MHC repertoire) suggests adaptation to stable, particle-rich anoxic niches where a reliable conductive scaffold is available, diminishing the need for alternative EET routes via cell surface proteins.

Together, these results provide the genomic blueprint of a naturally occurring microbial consortium obligately reliant on conductive particles. By extending conductive-particle-mediated syntrophy beyond synthetic dual-species laboratory models, we begin to grasp the ecological relevance of CIET in coastal sediments and beyond.

Implications

Long distance electron transfer in subsurface sediments has been proposed to operate as a directional chain of short-distance electron transfer-units[64]. The *Ca*. Geosyntrophus acetoxidans-*Methanosarcina* consortium described here exemplifies one such unit, with electrons flowing via conductive particles between the electrogenic SAO-bacterium and the electrotrophic methanogen, forming a particle-bound CIET module that can be embedded within larger redox-gradient electron transfer networks.

Geoconductors (conductive particles native to soils and sediments) are abundant in the very settings where our mechanisms should matter, anoxic soils and sediments[65–74]. Black carbon (BC), from wildfires, fossil fuel combustion and industrial sources can reach extreme levels near coastlines, glacier bays and river runoffs[65–74]. For example, BC reached up to 17 mg g^{-1} dry sediment in heavily polluted Norwegian harbors[75]; ~8 mg g^{-1} in some North American estuaries[76]; as much as ~100% of total organic carbon (TOC) in Arctic glacial bays (e.g., Kongsfjorden)[77] where BC-contaminated particulates are rapidly deposited at glacial fronts[77]; and up to 46 ± 2% of TOC in Baltic Sea river-outflow sediments[78], where our consortium is derived from. Beyond BC, iron-bearing geoconductors (magnetite, pyrite, greigite) are widespread[71,79,80]: iron is the fourth most abundant crustal element, and reactive, metastable Fe phases (e.g., ferrihydrite, goethite) are enriched in top sediment strata of coastal wetlands[71,79,80]. Rivers, atmospheric dust, and hydrothermal inputs continuously deliver these minerals and chars to coastal sediments, while climate-driven erosion[81,82], glacial melt, wildfires[66,74], coal combustion[83], supplementation in agriculture and other anthropogenic deposition increase geoconductor loads beyond natural levels.

These particle inventories provide persistent niches that may select for EET-enabled metabolisms and interspecies interactions. Such metabolisms are often overlooked in laboratory studies that rely on cells removed from their native matrices. Given the documented geoconductor abundance (black carbon and iron minerals like magnetite) in many coastal and estuary environments, particle-obligate syntrophies are likely important players in routing organics to methane. However, distinguishing particle-obligate syntrophy from other methanogenic pathways in situ remains challenging[4]. The genomic features identified here (PCC-clusters and MmcA variants) were consistently associated only with CIET consortia and could support the development of targeted detection approaches. It is now critical to (i) survey geoconductor-rich sites (e.g., harbors with BC ≳10 mg g^{-1}, polluted estuaries, Arctic glacial bays, Baltic river runoffs) for CIET-partnerships and CIET-SAO rates; (ii) establish thresholds for particle type, size, and conductivity that sustain CIET; and (iii) obtain in situ rate measurements to quantify the contribution of particle-mediated methanogenesis to methane budgets. Since eroded terrigenous inputs and anthropogenic deposition are increasing, quantifying when and where geoconductors support these alliances is essential for predicting methane emissions under accelerating environmental change.

Method

Cultivation

Over 9 years, we conducted routine biannual serial transfers, reaching 22 transfers during this study. Each transfer was initiated with 10% or 20% inoculum in fresh DSMZ modified 120 media[15], containing 10 mM acetate as the sole electron donor. Control incubations were prepared without conductive particles, while incubations with conductive particles received 10 g/L Granular Activated Carbon (GAC, Merck; <5 mm).

Before adding the sterile media and inoculum, GAC was wet presterilized. This was done by overlaying it with 200 μL of ultrapure water, then degassing it for 3 min with an 80:20 N_2:CO_2 gas mix and finally autoclaving it at 121 °C for 25 min. The media was autoclaved separately and then added to the bottles containing sterile GAC under strict anaerobic conditions[15].

The serum bottle volume for the inoculations was 100 mL, consisting of 50 mL culture and 50 mL headspace. All subsequent transfers were prepared in 50 mL blue chlorobutyl-rubber-stoppered glass vials. All culture experiments were carried out with at least three biological replicates.

All cultures were incubated in the dark, without shaking, at room temperature (22 °C). Subsampling and transfer procedures were performed under strict sterile and anaerobic conditions using gas-tight syringes and hypodermic needles degassed with an 80:20 N_2:CO_2 gas mix.

Analytical measurements

For methane determination, headspace gas (1 mL) was sampled at the time points shown in Fig. 1 (days 0, 14, 21, 28, 35, 42) using sterile, degassed syringes and injected using the gas displacement method in 3 mL gas-tight exetainers (Labco, UK) filled with sterile water (Yee et al.[25]). These methane samples were stored upside down at room temperature until measurement. Headspace methane concentrations were determined by injecting 100 μL in a Trace 1300 gas chromatograph (Thermo-Scientific) equipped with a TG-Bond Msieve 5A column (30 m × 0.53 mm × 50 μm) and a flame ionization detector. Nitrogen was used as the carrier gas at 5 mL/min flow rate. The oven was maintained at an isothermal temperature of 150 °C, while the injector

and detector temperatures were set at 200 °C. Methane quantification was based on external calibration using *in-house* prepared gas standards, ranging from 0.01 to 20% CH_4 in CO_2. To determine the acetate concentration in the media, we sampled 1 mL of media with a 1 mL gas-tight syringe, filtered through a 0.45 μm filter, and diluted 1:10 with ultrapure water. Acetate samples were then measured on a Dionex ICS-1500 Ion Chromatography System (ICS-1500) equipped with the AS50 autosampler, and an IonPac AS22 column coupled to a conductivity detector (31 mA). The eluent used was 4.5 mM Na_2CO_3 with 1.4 mM $NaHCO_3$, and the run was isothermic at 30 °C with a flow rate of 1.2 mL/min[26].

Helium ion microscopy

To investigate the spatial distribution of the microorganisms on the GAC surface, we examined the microorganisms attached to it using Scanning Helium Ion Microscopy (HIM). The samples were fixed overnight, in the dark at 4 °C, using a solution of 2.5% glutaraldehyde in 0.1 M phosphate buffer (pH 7.3). After fixation, the samples were washed three times in 0.1 M phosphate buffer for 10 min each, followed by a dehydration process through a graded series of ethanol (50%, 70%, 80%, 90%, 95%, and 100%) with each concentration being used three times for 10 min each[84]. Subsequently, the samples were immersed twice in pure hexamethyldisilazane for 30 s and then air-dried for 10 min[85]. Imaging was conducted using a Zeiss ORION NanoFAB Helium Ion Microscope with secondary electron (SE) detection (Zeiss, Germany). Helium ion imaging was performed at 30 keV beam energy, with a probe current ranging from 0.129 to 0.152 pA and a scan dwell time of 1 μs. Charge compensation was applied when necessary, using a low-energy electron flood gun (433 eV), and the working distance during imaging ranged from 8.0 to 8.8 mm. HIM images were manually colorized post-acquisition in BioRender to enhance visual distinction between cells and the carbon background.

DNA extraction and sequencing

DNA was extracted from a parallel set of GAC incubations when methane production reached mid-exponential (2 mM, at day 42) and from particle-free control incubations on day 42. DNA was purified using the DNeasy PowerLyzer PowerSoil Kit (Qiagen). The extraction process followed a modified manufacturer's protocol, which included specific centrifugation and resuspension steps. For bead beating, we used G2 DNA/RNA Enhancer beads 0.1 mm (A420150) for varying durations based on the sample type GAC samples for 7.5 min, and GAC-free control samples for 3 min. The concentrations and purities of the DNA were measured with the Qubit dsDNA HS Assay kit (Thermo Fisher Scientific, USA) and NanoDrop One (Thermo Fisher Scientific, USA). DNA size distributions were evaluated using the Genomic DNA ScreenTapes on the Agilent Tapestation 4200 (Agilent, USA). Nanopore sequencing was performed by DNASense (Aalborg, Denmark). In brief, barcoded SQK-NBD114.96 (AC-C, AC-MGN) and SQK-RPB114.24 (AC-GAC) DNA libraries were prepared according to the manufacturer's protocol, except for minor modifications (Oxford Nanopore Technologies, Oxford, United Kingdom). The barcoded DNA libraries were loaded onto primed FLO-PRO114M (R10.4.1) flow cells and sequenced on a PromethION P2 Solo device, running MinKNOW Release 23.07.12. Signal data was base called and demultiplexed with Dorado basecall server v. 7.1.4 (Oxford Nanopore Technologies, Oxford, United Kingdom) using the super-accurate algorithm (dna_r10.4.1_e8.2_400bps_5khz_sup.cfg). The remaining adapters were trimmed with Porechop v. 0.2.4. Removal of low-quality reads and generation of basic sequencing data statistics were obtained using Nanoqv. 0.10.0[86].

De novo assembly, binning and annotation

De novo assemblies were generated by DNASense (Aalborg, DK) individually for GAC and GAC-free control samples with Flye v. 2.9.2-b1786[87–89], setting the flags –meta and–extra-params min_read_cov_cutoff=10. The draft assembly was subsequently polished once with Medaka v. 1.8.0 (Oxford Nanopore Technologies, Oxford, United Kingdom). Assembly graphs were inspected with Bandage v. 0.8.1[90]. Contigs below 1000 bp were removed with SeqKit v. 2.2.0[91]. Contigs were subjected to automated binning using MetaBAT2 v. 2.15[92,93]. Intra-assembly MAG filtering and inter-assembly MAG dereplication were conducted using dRep v. 3.4.3, setting minimum MAG length (cluster size) to 0.5 Mbp, minimum completion to 1% and maximum contamination to 10% thresholds[94]. MAG completeness and contamination levels were assessed using CheckM2 v. 1.0.1[95,96]. MAG abundances were calculated using CoverM v. 0.6.1, setting –min-read-percent-identity 95 and –min-read-aligned-percent 90.

The final MAGs were classified against the GTDB release 214 using the GTDB toolkit v. 2.3.0[97]. Quality filtered DNA sequencing reads were classified with Kaiju v. 1.9.2, against the nr_euk 2023-05-10 database (321 mio. protein sequences from both prokaryotes, microbial eukaryotes and viruses)[98]. Filtered ONT fastq reads were converted to fasta using GNU Awk v. 5.0.1, and genes encoding rRNA were extracted with Barrnap v. 0.9 using a bacterial hidden Markov model. The SILVA 16S/18S rRNA 138 SSURef NR99 full-length database in RESCRIPt format was downloaded from the QIIME on 29 September 2022[99–101]. Potential generic placeholders and dead-end taxonomic entries were cleared from the taxonomy flat file, i.e., entries containing uncultured or unassigned metagenomes, were replaced with a blank entry. Extracted rRNA genes were mapped to the database using Minimap2 v. 2.24-r1122[102] and sorted using Samtools v.1.15.1[103]. Mapping results were filtered such that alignment sequence length covered >85% of database entry, and with mapping quality score >0.85. Further bioinformatic processing was done via RStudio IDE (2022.12.0.353) running R version 4.2.2 (2022-10-31 ucrt) and using the R packages: ampvis2[104], tidyverse (2.0.0), seqinr, ShortRead and iNEXT[105,106]. Bakta v. 1.8.1[107] and Prokka v. 1.14.6[108] were used to annotate the dereplicated bacteria and archaea MAGs using the –compliant flag (Genbank/ENA/DDJB compliance), respectively. The –skip-crispr flag was envoked in Bakta.

Phylogenomics trees

For phylogenomic analysis of the *Ca*. *Geosyntrophus acetoxidans* and the Baltic *Methanosarcina*, we used bacterial and archaeal marker gene sets provided by the Genome Taxonomy Database (GTDB; release R214), comprising 120 bacterial marker genes (bac120) and 53 archaeal marker proteins (arch53).

The precomputed alignments for the bac120 dataset were downloaded from the PhyloM.bac120.aln directory, with each marker gene aligned up to ~1052 bacterial reference genomes. From NCBI, we downloaded amino acid sequences from the type strains of representatives within the *Geobacteraceae* and made our database, including our own *Ca*. Geosyntrophus acetoxidans and *Geobacter psychrophilus* P39 genomes. Using BLASTP, searches were performed with the following parameters: BLOSUM62 scoring matrix, gap costs of 11 (open) and 1 (extend), *E*-value threshold of $1e^{-10}$, and a maximum of 5 hits per query. The top hit per genome (lowest *E*-value) was selected for further analysis, and the protein sequences were aligned using MAFFT[109]. Maximum likelihood phylogenetic trees were constructed with RAxML[110] and 100 bootstrap replicates. Phylogenomic inference was conducted using the PROTCAT model with the DAYHOFF substitution matrix, 25 rate categories, and default seed values (parsimony and bootstrap = 12345). Trees were visualized and annotated using iTOL v6[111].

The same workflow was applied to archaeal genomes affiliated with the genus *Methanosarcina*. For this, individual alignments of the 53 archaeal marker genes were obtained from the arch53/msa/individual directory of GTDB release R214.

EET-machinery identification, synteny and evolutionary relationships

All multiheme cytochromes were identified by accounting for all the heme-binding motifs in our MAGs using an in-house script that screened predicted proteins for the canonical CxxCH motif as well as non-canonical variants[40] (Supplementary Data Table S2). Each motif was searched separately, allowing for no mismatches. Subcellular localization of all identified multiheme cytochromes was predicted using PSortB vs. 3.0.3[112] and DeepLocPro vs.1.0[113]. Phyletic affiliation of all multiheme cytochromes in *Ca*. Geosyntrophus acetoxidans was determined by BLASTP searches against NCBI and OrthoDB and evolutionary rates were retrieved from OthoDB (Supplementary Data Table S2).

To determine OmcB evolutionary relationships, the *Ca*. Geosyntrophus OmcB sequence was used as a BLASTP query to identify homologs from related species. Top OmcB hits were collected and used to assemble a dedicated Geobacteraceae OmcB reference database. These protein sequences were aligned with MAFFT, and a maximum-likelihood tree was constructed using RaxML in Geneious v. 2025.2.1. A similar strategy was applied to resolve the evolutionary relationships of the MmcA heptaheme cytochrome from the Baltic *Methanosarcina* MAG.

To identify the porin–cytochrome–cytochrome (PCC) gene clusters, genomic regions upstream of successive multiheme cytochromes were manually inspected for porin genes. Upstream sequences were analyzed using InterPro (release 103.0) and porin domains were confirmed by detection of Superfamily SSF56935 (Model: 0048638) consistent with β-barrels proteins that cross the outer membrane acting as a pore[114]. Conserved gene organizations (synteny) of the PCC-clusters and other MHC-containing modules was assessed relative to the *Geobacter sulfurreducens* genome by evaluating gene order, orientation, gene content and presence or absence of homologous modules.

To identify putative electrically conductive e-pili, we used the e-pilin protein sequence from *Geobacter sulfurreducens* PCA (GenBank accession: AAR34870.1) as a reference[43]. This sequence was aligned against the *Ca*. Geosyntrophus acetoxidans MAG, and aromatic amino acid content and spacing were assessed following Walker et al.[43]. A comparable procedure was used to identify archaella proteins in the Baltic Methanosarcina MAG, using *flaB1* (WP_011023000.1) and *flaB2* (WP_011023001.1) of *M. acetivorans* CA2[44] as references.

Average nucleotide identity (ANI) and average aminoacid identity (AAI)

The genome wide ANI of *Ca*. Geosyntrophus acetoxidans and Baltic *Methanosarcina* was calculated against their closest relatives using OrthoANI Tool (OAT) from EYBiocloud[115]. OAT employs the OrthoANI algorithm and BLAST calculations to measure the similarity between two genome sequences.

For the calculation of the genome-wide AAI[116] between closest related proteomes, computed protein sequences were pairwise aligned using DIAMOND v2.0.15. Protein sequences from one genome were used to construct a searchable DIAMOND protein alignment database, and proteins from the second genome were queried against this database (and vice versa to identify reciprocal best hits, RBHs). Alignments were filtered using an *e*-value threshold of 1e−5, minimum sequence identity ≥30%, and minimum alignment length ≥50 amino acids. For each query protein, only the top-scoring hit (highest bit score; ties resolved by *e*-value) was retained. The genome-wide AAI was computed as the mean percentage identity across the filtered retained reciprocal best hits (RBHs).

Reporting summary

Further information on research design is available in the Nature Portfolio Reporting Summary linked to this article.

Data availability

The metagenome-assembled genomes (raw sequence data and assemblies) generated in this study have been deposited in the NCBI database under accession codes: Bioproject: PRJNA1140524. Biosamples: SAMN47284751 (GAC-incubations metagenome) SAMN47284749 (particle-free incubations metagenome) SAMN47284752 (whole-genome sequencing of *Geobacter psychrophilus* P39). For Baltic-Methanosarcina (GAC.MBAT.2) and *Ca*. Geosyntrophus acetoxidans (GAC.MBAT.93), protein-level homology searches were performed against well-annotated reference genomes: NC_002939.5 [https://www.ncbi.nlm.nih.gov/nuccore/NC_002939.5] (*Geobacter sulfurreducens* PCA) NC_003552.1 [https://www.ncbi.nlm.nih.gov/nuccore/NC_003552.1] (*Methanosarcina acetivorans* C2A) SAMN54926496 [https://www.ncbi.nlm.nih.gov/biosample/54926496] (GAC.MBAT.93, *Ca*. Geosyntrophus acetooxidans) SAMN54926476 [https://www.ncbi.nlm.nih.gov/biosample/54926476] (GAC.MBAT.2, Methanosarcina sp) All other analysis and data generated in this study are provided in the Supplementary Information or Source Data files. Source data are provided with this paper.

Materials availability

Cultures of the particle-dependent consortium are available from the corresponding author upon reasonable request, for research purposes that do not conflict with ongoing projects.

References

1. Forster, P. et al. The Earth's Energy Budget, Climate Feedbacks, and Climate Sensitivity. In *Climate Change 2021: The Physical Science Basis. Contribution of Working Group I to the Sixth Assessment Report of the Intergovernmental Panel on Climate Change* (eds Masson-Delmotte, V. et al.) 923–1054 (Cambridge University Press, Cambridge, United Kingdom and New York, NY, USA, 2021).
2. Mar, K. A., Unger, C., Walderdorff, L. & Butler, T. Beyond CO_2 equivalence: the impacts of methane on climate, ecosystems, and health. *Environ. Sci. Policy* **134**, 127–136 (2022).
3. Hattori, S. Syntrophic acetate-oxidizing microbes in methanogenic environments. *Microbes Environ.* **23**, 118–127 (2008).
4. Rotaru, A.-E., Yee, M. O. & Musat, F. Microbes trading electricity in consortia of environmental and biotechnological significance. *Curr. Opin. Biotechnol.* **67**, 119–129 (2021).
5. Petersen, S. P. & Ahring, B. K. Acetate oxidation in a thermophilic anaerobic sewage-sludge digestor: the importance of non-aceticlastic methanogenesis from acetate. *FEMS Microbiol. Lett.* **86**, 149–152 (1991).
6. Zinder, S. H. Syntrophic Acetate Oxidation and "Reversible Acetogenesis". in *Acetogenesis* 386–415. https://doi.org/10.1007/978-1-4615-1777-1_14 (Springer, 1994).
7. Zinder, S. H. & Koch, M. Non-aceticlastic methanogenesis from acetate: acetate oxidation by a thermophilic syntrophic coculture. *Arch. Microbiol.* **138**, 263–272 (1984).
8. Schnürer, A., Zellner, G. & Svensson, B. H. Mesophilic syntrophic acetate oxidation during methane formation in biogas reactors. *FEMS Microbiol. Ecol.* **29**, 249–261 (1999).
9. Hori, T., Noll, M., Igarashi, Y., Friedrich, M. W. & Conrad, R. Identification of acetate-assimilating microorganisms under methanogenic conditions in anoxic rice field soil by comparative stable isotope probing of RNA. *Appl Environ. Microbiol.* **73**, 101–109 (2007).
10. Liu, F. & Conrad, R. Thermoanaerobacteriaceae oxidize acetate in methanogenic rice field soil at 50 °C. *Environ. Microbiol.* **12**, 2341–2354 (2010).
11. Rui, J., Qiu, Q. & Lu, Y. Syntrophic acetate oxidation under thermophilic methanogenic condition in Chinese paddy field soil. *FEMS Microbiol. Ecol.* **77**, 264–273 (2011).

12. Karakashev, D., Batstone, D. J., Trably, E. & Angelidaki, I. Acetate oxidation is the dominant methanogenic pathway from acetate in the absence of Methanosaetaceae. *Appl. Environ. Microbiol.* **72**, 5138–5141 (2006).
13. Nüsslein, B., Chin, K.-J., Eckert, W. & Conrad, R. Evidence for anaerobic syntrophic acetate oxidation during methane production in the profundal sediment of subtropical Lake Kinneret (Israel). *Environ. Microbiol.* **3**, 460–470 (2001).
14. Zheng, S. et al. Co-occurrence of *Methanosarcina mazei* and Geobacteraceae in an iron (III)-reducing enrichment culture. *Front. Microbiol.* **6**, 941 (2015).
15. Rotaru, A.-E. et al. Conductive particles enable syntrophic acetate oxidation between *Geobacter* and *Methanosarcina* from coastal sediments. *mBio* **9**, e00226–18 (2018).
16. Owens, P. N. Soil erosion and sediment dynamics in the Anthropocene: a review of human impacts during a period of rapid global environmental change. *J. Soils Sediment.* **20**, 4115–4143 (2020).
17. Maher, B. A. & Taylor, R. M. Formation of ultrafine-grained magnetite in soils. *Nature* **336**, 368–370 (1988).
18. Mark Jensen, M., Thamdrup, B., Rysgaard, S., Holmer, M. & Fossing, H. Rates and regulation of microbial iron reduction in sediments of the Baltic-North Sea transition. *Biogeochemistry* **65**, 295–317 (2003).
19. Middelburg, J. J., Nieuwenhuize, J. & van Breugel, P. Black carbon in marine sediments. *Mar. Chem.* **65**, 245–252 (1999).
20. Marinho, B., Ghislandi, M., Tkalya, E., Koning, C. E. & de With, G. Electrical conductivity of compacts of graphene, multi-wall carbon nanotubes, carbon black, and graphite powder. *Powder Technol.* **221**, 351–358 (2012).
21. Schmidt, M. W. I. & Noack, A. G. Black carbon in soils and sediments: analysis, distribution, implications, and current challenges. *Glob. Biogeochem. Cycles* **14**, 777–793 (2000).
22. Rotaru, A.-E. et al. Interspecies interactions mediated by conductive minerals in the sediments of the iron rich meromictic Lake La Cruz, Spain. *Limnetica* **38**, 21–40 (2019).
23. Liu, F. et al. Promoting direct interspecies electron transfer with activated carbon. *Energy Environ. Sci.* **5**, 8982 (2012).
24. Rotaru, A.-E. et al. Direct interspecies electron transfer between *Geobacter metallireducens* and *Methanosarcina barkeri*. *Appl Environ. Microbiol* **80**, 4599–4605 (2014).
25. Yee, M. O., Snoeyenbos-West, O. L., Thamdrup, B., Ottosen, L. D. M. & Rotaru, A.-E. Extracellular electron uptake by two *Methanosarcina* species. *Front. Energy Res.* **7**, 29 (2019).
26. Yee, M. O. & Rotaru, A.-E. Extracellular electron uptake in Methanosarcinales is independent of multiheme c-type cytochromes. *Sci. Rep.* **10**, 372 (2020).
27. Rotaru, A.-E., Woodard, T. L., Nevin, K. P. & Lovley, D. R. Link between capacity for current production and syntrophic growth in *Geobacter* species. *Front. Microbiol.* **6**, 744 (2015).
28. Nevin, K. P. et al. *Geobacter bemidjiensis* sp. nov. and *Geobacter psychrophilus* sp. nov., two novel Fe(III)-reducing subsurface isolates. *Int. J. Syst. Evolut. Microbiol.* **55**, 1667–1674 (2005).
29. Parks, D. H. et al. A standardized bacterial taxonomy based on genome phylogeny substantially revises the tree of life. *Nat. Biotechnol.* **36**, 996–1004 (2018).
30. Xu, Z. et al. Genome-based taxonomic rearrangement of the order Geobacterales, including the description of *Geomonas azotofigens* sp. nov. and *Geomonas diazotrophica* sp. nov. *Front. Microbiol.* **12**, 737531 (2021).
31. Rodriguez-R, L. M. & Konstantinidis, K. T. Bypassing cultivation to identify bacterial species. *Microbe* **9**, 111–118 (2014).
32. Waite, D. W. et al. Proposal to reclassify the proteobacterial classes Deltaproteobacteria and Oligoflexia, and the phylum Thermodesulfobacteria into four phyla reflecting major functional capabilities. *Int. J. Syst. Evolut. Microbiol.* **70**, 5972–6016 (2020).
33. Lloyd, J. R. Microbial reduction of metals and radionuclides. *FEMS Microbiol. Rev.* **27**, 411–425 (2003).
34. Morgado, L., Bruix, M., Pessanha, M., Londer, Y. Y. & Salgueiro, C. A. Thermodynamic characterization of a triheme cytochrome family from *Geobacter sulfurreducens* reveals mechanistic and functional diversity. *Biophys. J.* **99**, 293–301 (2010).
35. Jiménez Otero, F., Chan, C. H. & Bond, D. R. Identification of different putative outer membrane electron conduits necessary for Fe(III) Citrate, Fe(III) Oxide, Mn(IV) oxide, or electrode reduction by *Geobacter sulfurreducens*. *J. Bacteriol.* **200**, https://doi.org/10.1128/jb.00347-18 (2018).
36. Liu, Y. et al. A trans-outer membrane porin-cytochrome protein complex for extracellular electron transfer by *Geobacter sulfurreducens* PCA. *Environ. Microbiol. Rep.* **6**, 776–785 (2014).
37. Soares, R., Fonseca, B. M., Nash, B. W., Paquete, C. M. & Louro, R. O. A survey of the Desulfuromonadia "cytochromome" provides a glimpse of the unexplored diversity of multiheme cytochromes in nature. *BMC Genom.* **25**, 982 (2024).
38. Rivas-Santisteban, J., Yubero, P. & Hurst, L. D. Cell compartment is a predictor of protein rate of evolution, but not in the manner expected: evidence against the extended complexity hypothesis. *Genome Biol. Evol.* **17**, evaf126 (2025).
39. Sojo, V., Dessimoz, C., Pomiankowski, A. & Lane, N. Membrane proteins are dramatically less conserved than water-soluble proteins across the tree of life. *Mol. Biol. Evol.* **33**, 2874–2884 (2016).
40. Soares, R., Costa, N. L., Paquete, C. M., Andreini, C. & Louro, R. O. A new paradigm of multiheme cytochrome evolution by grafting and pruning protein modules. *Mol. Biol. Evol.* **39**, msac139 (2022).
41. Wang, F. et al. Structure of microbial nanowires reveals stacked hemes that transport electrons over micrometers. *Cell* **177**, 361–369.e10 (2019).
42. Vargas, M. et al. Aromatic amino acids required for pili conductivity and long-range extracellular electron transport in *Geobacter sulfurreducens*. *mBio* **4**, e00105–e00113 (2013).
43. Walker, D. J. et al. Electrically conductive pili from pilin genes of phylogenetically diverse microorganisms. *ISME J.* **12**, 48–58 (2018).
44. Holmes, D. E., Zhou, J., Ueki, T., Woodard, T. & Lovley, D. R. Mechanisms for electron uptake by *Methanosarcina acetivorans* during direct interspecies electron transfer. *mBio* **12**, e02344–21 (2021).
45. Holmes, D. E. et al. Different outer membrane c-type cytochromes are involved in direct interspecies electron transfer to *Geobacter* or *Methanosarcina* species. *mLife* **1**, 272–286 (2022).
46. Zhuo, S. et al. The robustness of porin-cytochrome gene clusters from *Geobacter metallireducens* in extracellular electron transfer. *mBio* **15**, e00580–24 (2024).
47. Zhou, J., Holmes, D. E., Tang, H.-Y. & Lovley, D. R. Correlation of key physiological properties of *Methanosarcina* Isolates with environment of origin. *Appl Environ. Microbiol* **87**, e00731–21 (2021).
48. Rotaru, A.-E., Gharib, G., Jabaley, A., Anestis, K. & Kotoky, R. Cell surface differences within the genus *Methanosarcina* shape interactions with the extracellular environment. *J. Bacteriol.* **207**, e00112-25 (2025).
49. Gupta, D., Chen, K., Elliott, S. J. & Nayak, D. D. MmcA is an electron conduit that facilitates both intracellular and extracellular electron transport in *Methanosarcina acetivorans*. *Nat. Commun.* **15**, 3300 (2024).
50. Holmes, D. E. et al. Cytochrome-mediated direct electron uptake from metallic iron by *Methanosarcina acetivorans*. *mLife* **1**, 443–447 (2022).
51. Palacios, P. A., Snoeyenbos-West, O., Löscher, C. R., Thamdrup, B. & Rotaru, A.-E. Baltic Sea methanogens compete with acetogens for electrons from metallic iron. *ISME J.* **13**, 3011–3023 (2019).

52. Yi, Y. et al. Identification of novel butyrate- and acetate-oxidizing bacteria in butyrate-fed mesophilic anaerobic chemostats by DNA-based stable isotope probing. *Micro Ecol.* **79**, 285–298 (2020).
53. Obst, M., Krug, A., Luftmann, H. & Steinbüchel, A. Degradation of cyanophycin by *Sedimentibacter hongkongensis* strain KI and *Citrobacter amalonaticus* strain G isolated from an anaerobic bacterial consortium. *Appl. Environ. Microbiol.* **71**, 3642–3652 (2005).
54. Zhang, X., Mandelco, L. & Wiegel, J. *Clostridium hydroxybenzoicum* sp. nov., an amino acid-utilizing, hydroxybenzoate-decarboxylating bacterium isolated from methanogenic freshwater pond sediment. *Int J. Syst. Bacteriol.* **44**, 214–222 (1994).
55. Regueiro, L., Carballa, M. & Lema, J. M. Outlining microbial community dynamics during temperature drop and subsequent recovery period in anaerobic co-digestion systems. *J. Biotechnol.* **192**, 179–186 (2014).
56. Isaksen, M. F. & Teske, A. *Desulforhopalus vacuolatus* gen. nov., sp. nov., a new moderately psychrophilic sulfate-reducing bacterium with gas vacuoles isolated from a temperate estuary. *Arch. Microbiol.* **166**, 160–168 (1996).
57. Lie, T. J., Clawson, M. L., Godchaux, W. & Leadbetter, E. R. Sulfidogenesis from 2-aminoethanesulfonate (Taurine) fermentation by a morphologically unusual sulfate-reducing bacterium, *Desulforhopalus singaporensis* sp. nov. *Appl. Environ. Microbiol.* **65**, 3328–3334 (1999).
58. Sun, L. et al. Lentimicrobium saccharophilum gen. nov., sp. nov., a strictly anaerobic bacterium representing a new family in the phylum Bacteroidetes, and proposal of Lentimicrobiaceae fam. nov. *Int. J. Syst. Evol. Microbiol.* **66**, 2635–2642 (2016).
59. Zeng, Y. et al. Metabolism of novel potential syntrophic acetate-oxidizing bacteria in thermophilic methanogenic chemostats. *Appl. Environ. Microbiol.* **90**, e01090–23 (2024).
60. Zheng, D. et al. Identification of novel potential acetate-oxidizing bacteria in thermophilic methanogenic chemostats by DNA stable isotope probing. *Appl Microbiol. Biotechnol.* **103**, 8631–8645 (2019).
61. Rotaru, A.-E. et al. A new model for electron flow during anaerobic digestion: direct interspecies electron transfer to *Methanosaeta* for the reduction of carbon dioxide to methane. *Energy Environ. Sci.* **7**, 408–415 (2014).
62. Shi, L., Fredrickson, J. K. & Zachara, J. M. Genomic analyses of bacterial porin-cytochrome gene clusters. *Front. Microbiol.* **5**, 657 (2014).
63. Gonzalez, V. et al. Novel insights on extracellular electron transfer networks in the Desulfovibrionaceae family: unveiling the potential significance of horizontal gene transfer. *Microorganisms* **12**, 1796 (2024).
64. Zhang, Y. et al. Directional long-distance electron transfer from reduced to oxidized zones in the subsurface. *Nat. Commun.* **15**, 6576 (2024).
65. Yang, Z. et al. A coupled function of biochar as geobattery and geoconductor leads to stimulation of microbial Fe(III) reduction and methanogenesis in a paddy soil enrichment culture. *Soil Biol. Biochem.* **163**, 108446 (2021).
66. Zhang, C. et al. Pyrogenic carbon records of Holocene fire dynamics in the Yellow River Basin: climate change and human activity forcing. *Palaeogeogr. Palaeoclimatol. Palaeoecol.* **659**, 112626 (2025).
67. Dan, S. F. et al. Sources, burial flux and mass inventory of black carbon in surface sediments of the Daya Bay, a typical mariculture bay of China. *Mar. Pollut. Bull.* **179**, 113708 (2022).
68. Coppola, A. I. et al. The black carbon cycle and its role in the Earth system. *Nat. Rev. Earth Environ.* **3**, 516–532 (2022).
69. Yan, C. et al. Heterogeneous distributions of black carbon in sediments from three Asian mangrove wetlands. *Mar. Environ. Res.* **210**, 107323 (2025).
70. Zhang, Q. et al. Sources and dynamics of dissolved black carbon in the Pearl River Estuary and Shelf, Northern South China Sea. *J. Oceanogr.* **80**, 71–83 (2024).
71. Ma, H. et al. Enrichment of metastable iron minerals in global coastal wetlands. *Nat. Geosci.* 1–8. https://doi.org/10.1038/s41561-025-01764-7. (2025).
72. Laufer, K., Michaud, A. B., Røy, H. & Jørgensen, B. B. Reactivity of iron minerals in the seabed toward microbial reduction—a comparison of different extraction techniques. *Geomicrobiol. J.* **37**, 170–189 (2020).
73. Amiel, N., Shaar, R. & Sivan, O. The effect of early diagenesis in methanic sediments on sedimentary magnetic properties: case study from the SE Mediterranean continental shelf. *Front. Earth Sci.* **8**, 283 (2020).
74. Wagner, S. et al. Isotopic composition of oceanic dissolved black carbon reveals non-riverine source. *Nat. Commun.* **10**, 5064 (2019).
75. Oen, A. M. P., Breedveld, G. D., Kalaitzidis, S., Christanis, K. & Cornelissen, G. How quality and quantity of organic matter affect polycyclic aromatic hydrocarbon desorption from Norwegian harbor sediments. *Environ. Toxicol. Chem.* **25**, 1258–1267 (2006).
76. Mitra, S., Bianchi, T. S., McKee, B. A. & Sutula, M. Black carbon from the Mississippi River: quantities, sources, and potential implications for the global carbon cycle. *Environ. Sci. Technol.* **36**, 2296–2302 (2002).
77. Zaborska, A., Winogradow, A. & Burska, D. Contamination History of Soot Black Carbon in the Arctic, as Retrieved from Fjordic Sediments. SSRN Scholarly Paper at https://doi.org/10.2139/ssrn.4425556 (2023).
78. Staniszewska, M., Koniecko, I., Falkowska, L., Burska, D. & Kiełczewska, J. The relationship between the black carbon and bisphenol A in sea and river sediments (Southern Baltic). *J. Environ. Sci.* **41**, 24–32 (2016).
79. Canfield, D. E. & Berner, R. A. Dissolution and pyritization of magnetite in anoxie marine sediments. *Geochim. Cosmochim. Acta* **51**, 645–659 (1987).
80. Usman, M. et al. Magnetite and green rust: synthesis, properties, and environmental applications of mixed-valent iron minerals. *Chem. Rev.* **118**, 3251–3304 (2018).
81. Jørgensen, B. B., Laufer, K., Michaud, A. B. & Wehrmann, L. M. Biogeochemistry and microbiology of high Arctic marine sediment ecosystems—Case study of Svalbard fjords. *Limnol. Oceanogr.* **66**, S273–S292 (2021).
82. Neugebauer, I. et al. Preservation of Fe/Mn-redox fronts in sediments of an oligotrophic, oxygenated deep-water lake (Lago Fagnano, Tierra del Fuego). *Sedimentology* **69**, 1841–1860 (2022).
83. Li, Y., Guo, F., Yu, Y., Zhang, Z.-J. & Liu, J.-H. Control of atmospheric deposition and hydrodynamic conditions on black carbon distribution in coastal sediments. *Sci. Total Environ.* **978**, 179438 (2025).
84. Kawaichi, S., Kotoky, R., Fiutowski, J. & Rotaru, A.-E. Adaptation of a methanogen to Fe^0 corrosion via direct contact. *npj Biofilms Microbiomes* **10**, 100 (2024).
85. Araujo, J. C. Comparison of hexamethyldisilazane and critical point drying treatments for SEM analysis of anaerobic biofilms and granular sludge. *J. Electron Microsc.* **52**, 429–433 (2003).
86. Steinig, E. & Coin, L. Nanoq: ultra-fast quality control for nanopore reads. *J. Open Source Spftw.* **7**, 2991 (2022).
87. Kolmogorov, M. et al. metaFlye: scalable long-read metagenome assembly using repeat graphs. *Nat. Methods* **17**, 1103–1110 (2020).

88. Kolmogorov, M., Yuan, J., Lin, Y. & Pevzner, P. A. Assembly of long, error-prone reads using repeat graphs. *Nat. Biotechnol.* **37**, 540–546 (2019).
89. Lin, Y.-Y. et al. De novo assembly of highly polymorphic metagenomic data using in situ generated reference sequences and a novel BLAST-based assembly pipeline. *BMC Bioinform.* **18**, 1–10 (2017).
90. Wick, R. R., Schultz, M. B., Zobel, J. & Holt, K. E. Bandage: interactive visualization of de novo genome assemblies. *Bioinformatics* **31**, 3350–3352 (2015).
91. Shen, W., Le, S., Li, Y. & Hu, F. SeqKit: a cross-platform and ultrafast toolkit for FASTA/Q file manipulation. *PLoS ONE* **11**, e0163962 (2016).
92. Kang, D. D. et al. MetaBAT 2: an adaptive binning algorithm for robust and efficient genome reconstruction from metagenome assemblies. *PeerJ* **7**, e7359 (2019).
93. Nissen, J. N. et al. Improved metagenome binning and assembly using deep variational autoencoders. *Nat. Biotechnol.* **39**, 555–560 (2021).
94. Olm, M. R., Brown, C. T., Brooks, B. & Banfield, J. F. dRep: a tool for fast and accurate genomic comparisons that enables improved genome recovery from metagenomes through de-replication. *ISME J.* **11**, 2864–2868 (2017).
95. Chklovski, A., Parks, D. H., Woodcroft, B. J. & Tyson, G. W. CheckM2: a rapid, scalable and accurate tool for assessing microbial genome quality using machine learning. *Nat. Methods* **20**, 1203–1212 (2023).
96. Parks, D. H., Imelfort, M., Skennerton, C. T., Hugenholtz, P. & Tyson, G. W. CheckM: assessing the quality of microbial genomes recovered from isolates, single cells, and metagenomes. *Genome Res* **25**, 1043–1055 (2015).
97. Chaumeil, P.-A., Mussig, A. J., Hugenholtz, P. & Parks, D. H. GTDB-Tk: a toolkit to classify genomes with the Genome Taxonomy Database. *Bioinformatics* **36**, 1925–1927 (2020).
98. Menzel, P., Ng, K. L. & Krogh, A. Fast and sensitive taxonomic classification for metagenomics with Kaiju. *Nat. Commun.* **7**, 11257 (2016).
99. Quast, C. et al. The SILVA ribosomal RNA gene database project: improved data processing and web-based tools. *Nucleic Acids Res.* **41**, D590–D596 (2013).
100. Robeson, M. et al. RESCRIPt: Reproducible sequence taxonomy reference database management. *PLOS Comput. Biol.* **17**, e1009581 (2021).
101. Yilmaz, P. et al. The SILVA and "All-species Living Tree Project (LTP)" taxonomic frameworks. *Nucleic Acids Res* **42**, D643–D648 (2014).
102. Li, H. Minimap2: pairwise alignment for nucleotide sequences. *Bioinformatics* **34**, 3094–3100 (2018).
103. Li, H. et al. The sequence alignment/map format and SAMtools. *Bioinformatics* **25**, 2078–2079 (2009).
104. ampvis2: an R package to analyse and visualise 16S rRNA amplicon data | bioRxiv. https://www.biorxiv.org/content/10.1101/299537v1.abstract.
105. Chao, A., Chiu, C.-H. & Jost, L. Unifying species diversity, phylogenetic diversity, functional diversity, and related similarity and differentiation measures through hill numbers. *Annu. Rev. Ecol. Evol. Syst.* **45**, 297–324 (2014).
106. Hsieh, T. C., Ma, K. H. & Chao, A. iNEXT: an R package for rarefaction and extrapolation of species diversity (Hill numbers). *Methods Ecol. Evol.* **7**, 1451–1456 (2016).
107. Schwengers, O. et al. Bakta: rapid and standardized annotation of bacterial genomes via alignment-free sequence identification. *Microb. Genom.* **7**, 000685 (2021).
108. Seemann, T. Prokka: rapid prokaryotic genome annotation. *Bioinformatics* **30**, 2068–2069 (2014).
109. Katoh, K. & Standley, D. M. MAFFT multiple sequence alignment software version 7: improvements in performance and usability. *Mol. Biol. Evol.* **30**, 772–780 (2013).
110. Stamatakis, A. RAxML version 8: a tool for phylogenetic analysis and post-analysis of large phylogenies. *Bioinformatics* **30**, 1312–1313 (2014).
111. Letunic, I. & Bork, P. Interactive Tree Of Life (iTOL) v5: an online tool for phylogenetic tree display and annotation. *Nucleic Acids Res* **49**, W293–W296 (2021).
112. Yu, N. Y. et al. PSORTb 3.0: improved protein subcellular localization prediction with refined localization subcategories and predictive capabilities for all prokaryotes. *Bioinformatics* **26**, 1608–1615 (2010).
113. Nielsen, H. Practical applications of language models in protein sorting prediction: SignalP 6.0, DeepLoc 2.1, and DeepLocPro 1.0. in *Large Language Models (LLMs) in Protein Bioinformatics* 153–175. https://doi.org/10.1007/978-1-0716-4623-6_10 (Humana, 2025).
114. Paysan-Lafosse, T. et al. InterPro in 2022. *Nucleic Acids Res.* **51**, D418–D427 (2023).
115. Lee, I., Ouk Kim, Y., Park, S.-C. & Chun, J. OrthoANI: an improved algorithm and software for calculating average nucleotide identity. *Int. J. Syst. Evolut. Microbiol.* **66**, 1100–1103 (2016).
116. Gerhardt, K. et al. FastAAI: efficient estimation of genome average amino acid identity and phylum-level relationships using tetramers of universal proteins. *Nucleic Acids Res.* **53**, gkaf348 (2025).

Acknowledgements

This work contributes to a Danish Research Council grant DFF Project 2 (grant-number 1026-00159B) awarded to A.-E.R. Additional support was provided by MIMET, an ERC Consolidator Grant (grant-number 101045149) to A.-E.R. The microscopy imaging was supported by the Interreg 6a Deutschland-Denmark Program project PlastTrack (grant number 07-1-22 1) awarded to J.F. and by NANOCHEM (UFM5229-0001B) a National Infrastructure grant, represented in this work by J.F.

Author contributions

A.-E.R. and D.J. conceived and designed the study. D.J. performed experiments. D.J. and J.F. performed microscopy. D.J. and K.A. performed bioinformatic analysis with support from A.-E.R. A.-E.R., B.B.J., and K.U.K. acquired funding. A.-E.R. administered the project and provided resources (conductive particle dependent enrichments and strains). D.J., K.A., and A.-E.R. wrote the manuscript with input from all co-authors. All authors reviewed and approved the final manuscript.

Competing interests

The authors declare no competing interests.

Additional information

Supplementary information The online version contains supplementary material available at https://doi.org/10.1038/s41467-026-70468-2.

Correspondence and requests for materials should be addressed to Amelia-Elena Rotaru.

Peer review information *Nature Communications* thanks Lotta Purkamo and the other anonymous reviewer(s) for their contribution to the peer review of this work. A peer review file is available.